www.sciencemag.org/cgi/content/full/science.aae0328/DC1

Supplementary Materials for

Discovery of the interstellar chiral molecule propylene oxide (CH_3CHCH_2O)

Brett A. McGuire,* P. Brandon Carroll,* Ryan A. Loomis, Ian A. Finneran, Philip R. Jewell, Anthony J. Remijan, Geoffrey A. Blake

*Corresponding author. Email: bmcguire@nrao.edu (B.A.M.); pcarroll@caltech.edu (P.B.C.)

Published 14 June 2016 on *Science* First Release
DOI: 10.1126/science.aae0328

This PDF file includes:

Materials & Methods

Observations

The full observational details, data reduction strategy, and analysis of the PRIMOS observations presented here have been previously reported (*13*), and will not be discussed further. PRIMOS provides near-continuous frequency coverage of Sgr B2(N) from 1 – 50 GHz at high sensitivity (RMS$\sim$3 – 9 mK) and spectral resolution ($\Delta\nu \sim 25$ kHz) using the 100-m Robert C. Byrd Green Bank Telescope (GBT). PRIMOS data are fully-reduced and made publicly available with no propriety period. More information on how to obtain full data sets is available online at http://www.cv.nrao.edu/$\sim$aremijan/PRIMOS/, and large portions of the survey, as well as many others, are available through the **S**pectral **Li**ne **S**earch **E**ngine (SLiSE) at http://www.cv.nrao.edu/$\sim$aremijan/SLiSE/. Additionally, several hours of archival GBT observations (GBT Project AGBT06B-006) fortuitously covered the 12.8 GHz transition of propylene oxide. These data were reduced in the same way as the PRIMOS data, and used to further bolster the signal-to-noise of the line.

Observations with the Parkes Radio Telescope were conducted over a total of 9 nights from 30 April 2015 – 19 May 2015. The target coordinates for the observations were the same as those for the PRIMOS observations: right ascension = $17^h47^m19.8^s$, declination = -28°22′17.0″ (J2000). Spectra were acquired in position-switching mode, with the off-position located 1° offset in latitude with a switching cycle of 5 minutes. Pointing accuracy was checked by facility staff and converged to $\sim$5″ accuracy. The Parkes K_u-band receiver was used with a system temperature of $\sim$80 K across the band. The backend was an 8 MHz bandwidth, 1 kHz resolution Digital Filter Bank.

The quasar ICRF J193925.0-634245 was used for absolute flux calibration. Scans were collected in dual-polarization mode; these were averaged to increase the sensitivity of the ob-

servations. Background flux was removed from the scans using a 5th-order polynomial fit to the baseline. The resulting spectra were then binned and Hanning smoothed to a resolution of $\sim$0.6 km s^{-1}. Finally, an instrumental noise feature, or 'birdy,' was removed at $\sim$12069.8 MHz.

For such weak features there is a possibility that even small systematic response (e.g. standing waves) may obscure or even be mistaken for genuine molecular absorption. In order to ensure all absorption features were real, each feature was re-observed at a shifted rest frequency such that the target frequency was shifted within the passband. For Parkes observations, these tests were carried out concurrently with the observations described above in the same manner. The additional GBT observations were carried out over four sessions from 20 August 2015 – 16 September 2015 (GBT project AGBT15A-493). Observations were conducted in position-switching mode, with the off-position located 1° offset in azimuth with a switching cycle of 4 minutes. Pointing accuracy was checked and corrected every $\sim$ 2 hrs using the nearby continuum source PKSJ 1833-2103. The $2_{11} - 2_{02}$ and $3_{12} - 3_{03}$ lines were observed simultaneously using the GBT K_u-band receiver and the VEGAS spectrometer in its 187.5 MHz bandwidth mode. For both Parkes and GBT observations, the targeted transition(s) were successfully reproduced, and were appropriately shifted within the passband. Therefore, the features cannot be attributed to IF or passband response, and must be from the target source at the specified rest frequencies.

Laboratory Spectroscopy

The cm-wave spectrum of propylene oxide is complicated by coupling of the internal rotation of the methyl group to the overall rotation of the molecule. This splits each rotational level into a non-degenerate A state and a doubly degenerate E state. The high barrier to internal rotation (2710 cal/mole; 0.1175 eV) produces small splittings, $\sim$ 100 kHz, for low J transitions such as those observed here. These internal rotation-driven splittings will be unresolved for

astronomical observations toward Sgr B2(N), but will contribute appreciably to the observed line width. The pure rotational spectrum of propylene oxide has been previously measured and assigned (*27, 28*). However, due to linewidth and resolution limits in this (previous) work, the treatment of the splittings was insufficient for determining the contribution of this splitting to the astronomical linewidth. We have therefore re-measured these spectra using a state-of-the-art free jet microwave spectrometer.

Specifically, laboratory spectra were collected from 8–18 GHz using a direct digital synthesis (DDS)-based, chirped-pulse Fourier transform microwave (CP-FTMW) spectrometer. Details of the instrument have been published elsewhere (*29*). Briefly, a linear frequency sweep (0 – 2 GHz, 1 μs duration) chirped pulse is generated by a DDS card. This pulse is then upconverted by mixing with a local oscillator (8–18 GHz), amplified (to 50 W), and broadcast by a waveguide horn into the chamber to interact with the sample. Propylene oxide, sometimes referred to as methyl oxirane, (>99% purity), was purchased from Alfa Aesar, and used without further purification. The sample was prepared by flowing 1 atm of Ar through a sealed reservoir containing $\sim$5 mL of propylene oxide, and introduced into the vacuum chamber through a pulsed adiabatic expansion.

After excitation by the microwave pulse, the weak molecular free induction decay (FID) was collected using the same microwave horn, amplified (+38 dB), downconverted, and recorded with a high speed digital-to-analog converter (4 GSa/s). The expansion coupled with the coaxial excitation-detection geometry employed produces a rotationally cold ($\sim$3 K) gas with a slight asymmetry in the blended Doppler doublet. This limits the frequency uncertainty in the measured line centers to 20 kHz.

The use of the same local oscillator (LO) for both up and downconversion gives double sideband spectra, thus the absolute the frequency of any emission cannot be determined from a single scan. To determine absolute frequencies, a second scan is recorded at a slightly shifted

(LO+10 MHz) LO frequency. The deconvolved broadband spectrum is shown in Figure S1 using a 10 microsecond FID. To resolve the A-E splitting, we followed up with targeted measurements using a 130 microsecond FID (Figure S2). Each peak is a doublet of doublets; the A-E methyl rotor splitting is $\sim$100 kHz, while the Doppler splitting from the jet expansion is $\sim$50 kHz. Fit frequencies are given in Table S1.

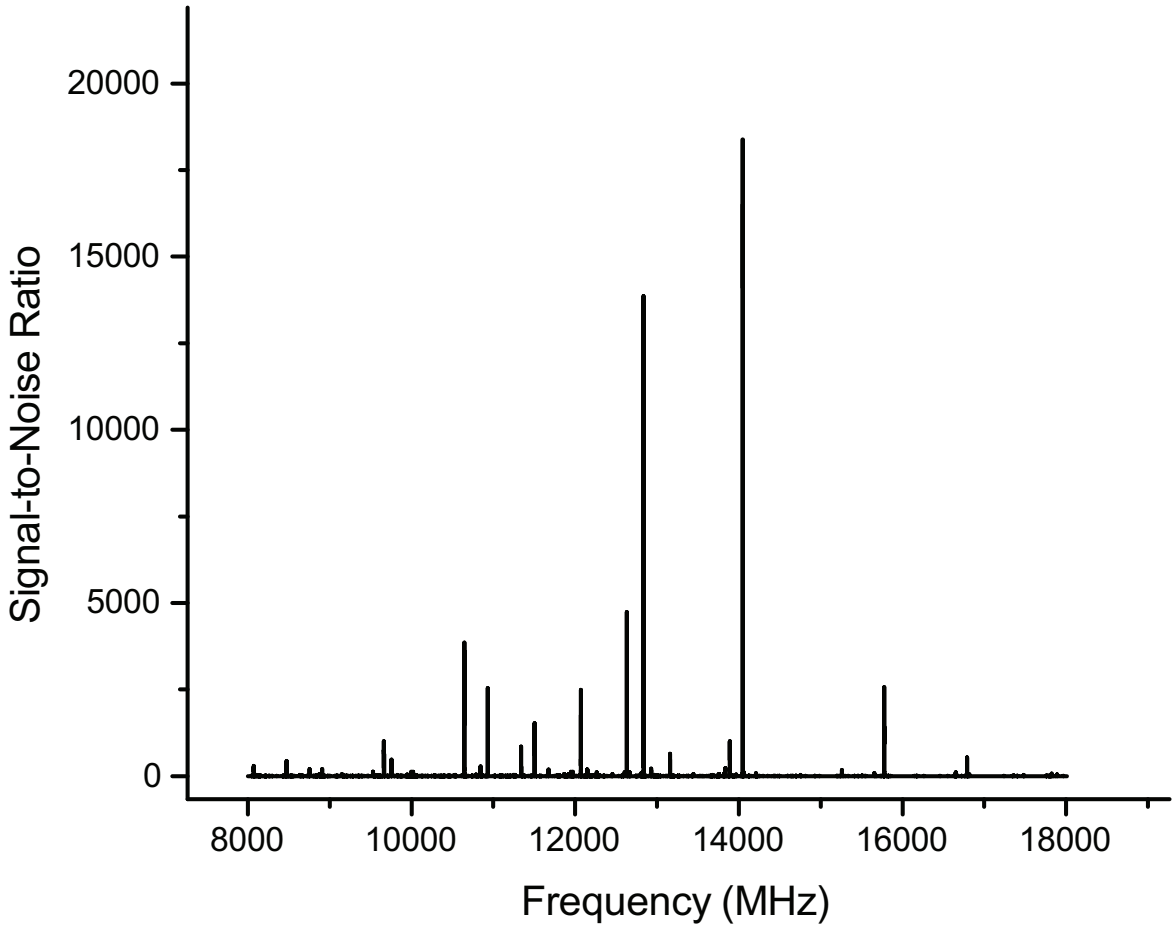

Figure S1. Laboratory spectrum of propylene oxide. The spectrum of propylene oxide in an Ar buffer gas from 8 – 18 GHz (4.8 million averages, 20 hour acquisition)

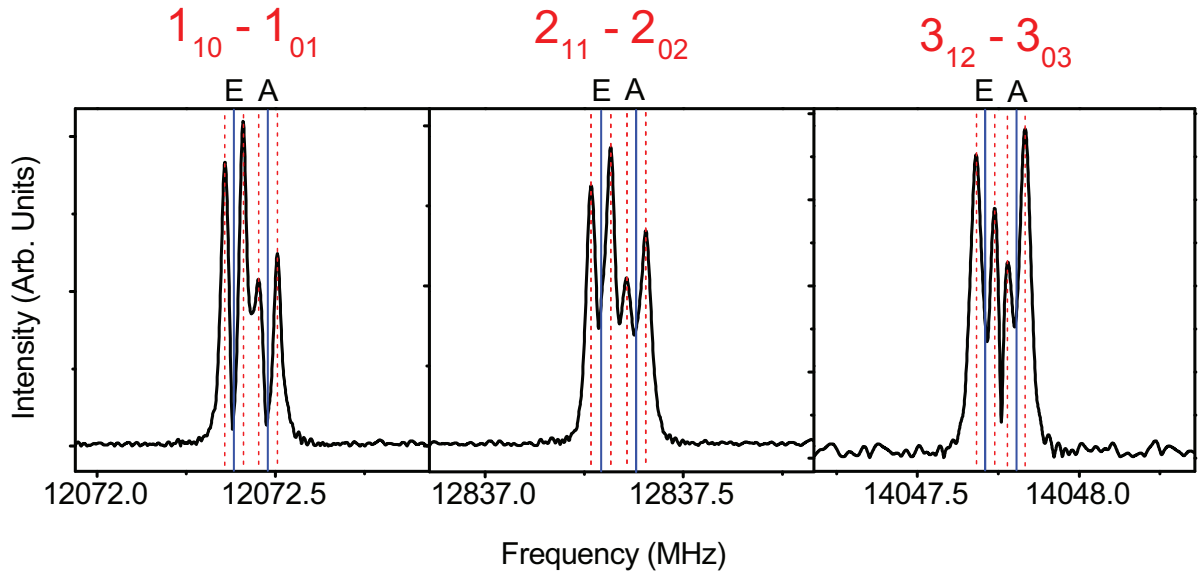

Figure S2. Laboratory spectra of astronomically-observed propylene oxide transitions. Laboratory measurement of the three transitions detected astronomically in this work, showing the characteristic A-E methyl rotor splitting (solid blue lines) and Doppler splitting (dashed red lines). Rotational quantum numbers are given in red.

Table S1. Measured laboratory frequencies of the transitions used in this work, and associated observed linewidth broadening.

$J'_{K_aK_c} - J''_{K_aK_c}$	Symmetry	Frequency (MHz)	ΔV (km s^{-1})
$1_{10} - 1_{01}$	E	12072.384(20)	2.4
	A	12072.479(20)	
$2_{11} - 2_{02}$	E	12837.292(20)	2.1
	A	12837.381(20)	
$3_{12} - 3_{03}$	E	14047.715(20)	1.9
	A	14047.806(20)	

The Observational Model

To determine a column density and rotational temperature for propylene oxide, we follow the convention of (*11*), using Equation 1 to calculate the column density N_T, given a rotational partition function Q_r, upper state energy E_u, rotational excitation temperature T_{ex}, transition frequency ν, line strength $S\mu^2$, observed intensity ΔT_A^*, linewidth ΔV, telescope efficiency η_B, and background temperature T_{bg}.

$$N_T = \frac{Q_r e^{E_u/kT_{ex}}}{\frac{8\pi^3}{3k}\nu S\mu^2} \times \frac{\frac{1}{2}\sqrt{\frac{\pi}{ln(2)}}\frac{\Delta T_A^* \Delta V}{\eta_B}}{1 - \frac{e^{h\nu/kT_{ex}-1}}{e^{h\nu/kT_{bg}-1}}} \tag{1}$$

We make the assumption that all propylene oxide states can be described by a single excitation temperature equal to T_{ex}. We stress that this assumption does not imply that the molecule is necessarily in thermal equilibrium with the gas; T_{ex} is not assumed to be equal to the ambient gas kinetic temperature, a condition often described as Local Thermodynamic Equilibrium, or LTE. The excitation of molecules in Sgr B2(N), especially those in the cold absorbing layer(s) as is propylene oxide, rarely can be described by the gas kinetic temperature; yet, a single-excitation model often describes such species well (*11, 16, 30*).

The rotational partition function, Q_r, is often calculated according to a high-temperature approximation, given by Equation 2 where σ is a unitless symmetry parameter, T_{ex} the excitation temperature (K), and A, B, and C, the rotational constants of the molecule (MHz) (c.f. (*31*)), which offers excellent values down to modestly-low temperatures.

$$Q_r = \left(\frac{5.34 \times 10^6}{\sigma}\right)\left(\frac{T_{ex}^3}{ABC}\right)^{1/2} \tag{2}$$

Molecules seen in absorption toward Sgr B2(N), however, often are characterized by T_{ex} values as low as 6–8 K (*11, 32*), in which case direct summation of the energy levels is required, as

given in Equation 3 (c.f. (*31*)).

$$Q_r = \frac{1}{\sigma} \sum_{J=0}^{J=\infty} \sum_{K=-J}^{K=J} (2J+1) e^{-E_{J,K}/kT_{ex}} \tag{3}$$

For asymmetric molecules like propylene oxide, the symmetry parameter $\sigma = 1$. In this study, we directly sum the rotational states using Equation 3 to determine Q_r, however, we note that at the temperatures under consideration, the error in Equation 2 is only 1.3% at 6 K and drops below 0.1% by 40 K.

The $S\mu^2$ value is the intrinsic line strength S_{ij} multiplied by the square of the transition dipole moment μ, which in the case of the pure rotational transitions considered here is simply the permanent electric dipole moment μ along the principal axis of the transition. The S_{ij} factors are intrinsic quantum mechanical properties determined from the J and K values of the transition; a thorough reference tabulation is available (*33*). The dipole moments μ_a, μ_b, and μ_c were taken from (*27*) as 0.95, 1.67, and 0.56 Debye, respectively.

The observed intensities, ΔT_A^*, and linewidths, ΔV, were obtained by fitting a single Gaussian lineshape to the observed transitions (for PRIMOS observations), or a pair of Gaussians (for Parkes observations). In either case, the observed signals are well-fit. The results are given in Table S2. Given the uncertainties, we adopted a uniform linewidth of 13 km s^{-1} when considering the PRIMOS transitions. We note a trend of decreasing linewidth with increasing frequency, which we attribute to a combination of the decreasing beam size encompassing less inhomogeneous environments, and the decreasing broadening due to internal rotation as J-values increase.

The lines were fit, and the column density and temperature determinations conducted, using the laboratory frequencies (ν) determined without explicitly treating the splitting of the rotational levels due to internal motion because the splitting is not resolved in our observations. This splitting does, however, contribute a non-negligible amount to the total linewidth of the

Table S2. Line parameters resulting from Gaussian Fits to the observed transitions. Numbers in parenthesis are 1σ standard deviations in units of the last significant digit.

	Component 1			Component 2		
Transition	v_o (km s^{-1})	ΔT_A^* (mK)	ΔV (km s^{-1})	v_o (km s^{-1})	ΔT_A^* (mK)	ΔV (km s^{-1})
$1_{1,0} - 1_{0,1}$	59.3(18)	-45(3)	19.6(33)	45.5(23)	-13(9)	9.9(57)
$2_{1,1} - 2_{0,2}$	61.4(7)	-7.4(5)	15.8(20)	...	...	...
$3_{1,2} - 3_{0,3}$	63.0(8)	-6.8(6)	11.6(14)	...	...	...

observed features: 2.4, 2.1, and 1.9 km s^{-1} at 12.1, 12.8, and 14.0 GHz, respectively.

The telescope beam efficiency (η_b) was calculated explicitly at each frequency across the PRIMOS band using Equation 4 (c.f. (*34*)).

$$\eta_b = -15.52 \times 10^{-5}\nu^2 - 22.59 \times 10^{-4}\nu + 0.98 \tag{4}$$

As we also include the observations of (*10*) in our analysis, which were acquired with the MOPRA telescope, we take an average value of $\eta_b = 0.44$ uniformly across the 3 mm MOPRA observational window (*35*).

The background temperature (T_{bg}) plays a critical role in the accurate modeling of molecular excitation for transitions searched for in the PRIMOS observations, in particular for those molecules which are seen in absorption. This is readily apparent if Equation 1 is re-stated as Equation 5, below (c.f. (*11*)).

$$N_T = \frac{Q_r \frac{1}{2}\sqrt{\frac{\pi}{ln(2)}}\frac{\Delta T_A^* \Delta V}{\eta_B}}{\frac{8\pi^3}{3h}(T_{ex} - \frac{T_{bg}}{\eta_B})S\mu^2(e^{-E_l/kT_{ex}} - e^{-E_u/kT_{ex}})} \tag{5}$$

Here, it is clear from the $T_{ex} - \frac{T_{bg}}{\eta_B}$ term that for values of $T_{ex} < T_{bg}$, T_A^* must be negative (in absorption) for N_T to remain positive. As the observed propylene oxide transitions are in absorption, it is therefor critical to constrain T_{bg} in Sgr B2(N) at the frequencies observed. In this case, a model must first be adopted to describe the overlap of the GBT beam with the background continuum emission structure at each frequency.

The structure of Sgr B2(N) is complex, with a compact ($\sim 5''$) hot molecular core surrounded by a more extended, colder molecular shell (*34*). The background continuum structure against which molecules in this shell absorb is $\sim 20''$ in diameter (see, e.g., Fig. $3b$ of (*36*)). For the purposes of this study, we assume this $20''$ source size for the cold molecular material, and explicitly calculate the spatial overlap of these regions with the GBT beam as its size varies across the frequency coverage. The geometry-corrected source size is then used to determine a correction factor (B) to observed intensities for beam dilution effects, according to Equation 6, where θ_s and θ_b are the source and beam sizes, respectively. This is then applied as required to both peak line intensities (ΔT_A^*) and to the background continuum levels, as described below.

$$B = \frac{\theta_s^2}{\theta_s^2 + \theta_b^2} \tag{6}$$

The background continuum temperature at 85 points across the PRIMOS frequency coverage was established by (*34*). These continuum measurements range from more than 100 K at low frequencies to several Kelvin above the CMB near 45 GHz, although these measurements are not corrected for any assumed source geometry or beam dilution effects. The authors attribute this to non-thermal continuum in the source. We adopt their measurements of the continuum for these calculations, but correct them for the overlap of the assumed source size of the continuum-emitting region with the GBT beam in the PRIMOS observations. We expect this correction to be valid to frequencies as low as $\sim$10 GHz, below which the GBT beam is sufficiently large that it will encompass additional emitting regions. At that point, the beam dilution correction factor used here will no longer account for the full size of the emitting regions within the beam, and the continuum will be over-estimated in increasing degree.

The effect of this frequency-dependent continuum on the observed intensities of transitions, both in emission and in absorption, is significant. While the relative populations of the energy levels for a molecule at a single excitation temperature are still described by a Boltzmann dis-

tribution, the observed relative intensities of the transitions between those levels are not. This is most straightforward to understand looking at absorption transitions. The standard analysis of relative intensities from a molecule whose population is described by a Boltzmann distribution at a single excitation temperature provides predicted absorption depths (i.e. percent absorption). The measured (observed; ΔT_A^*) value is not, however, directly comparable, as the background against which a 10% absorptive transition at 45 GHz is absorbing is not the same as the background against which a 1% absorptive transition at 10 GHz is absorbing. Thus, the predicted absolute absorption spectrum for propylene oxide in the PRIMOS observations will present different relative intensities between transitions, due to this non-constant background, than a simple percentage absorption spectrum.

Model Results

Using the model described above, we have performed a least-squares analysis of our data, taking into account the two observed transitions in PRIMOS, all transitions covered by PRIMOS but for which no features are seen, as well as those transitions in the coverage of the survey conducted by (*10*). Due to the large difference beam size, telescope-specific parameters, receiver efficiencies, and calibration uncertainties, the Parkes transition was not included in the analysis quantitatively. The results of the analysis provide a set of models for column density and temperature which are consistent with our observations, meaning that given the frequency coverage and sensitivity of the PRIMOS observations and those of (*10*), only the transitions we have detected are expected to be present above the noise level of the observations. The best-fit model for the datasets, including both detected and non-detected lines in the PRIMOS observations and those of (*10*), is for a column density of 1×10^{13} cm^{-2} and an excitation temperature of $T_{ex} = 5.2$ K. A simulated spectrum under these conditions is shown in Figure S3, while insets (a) and (b) show simulations of the model overlaid on the observational spectra.

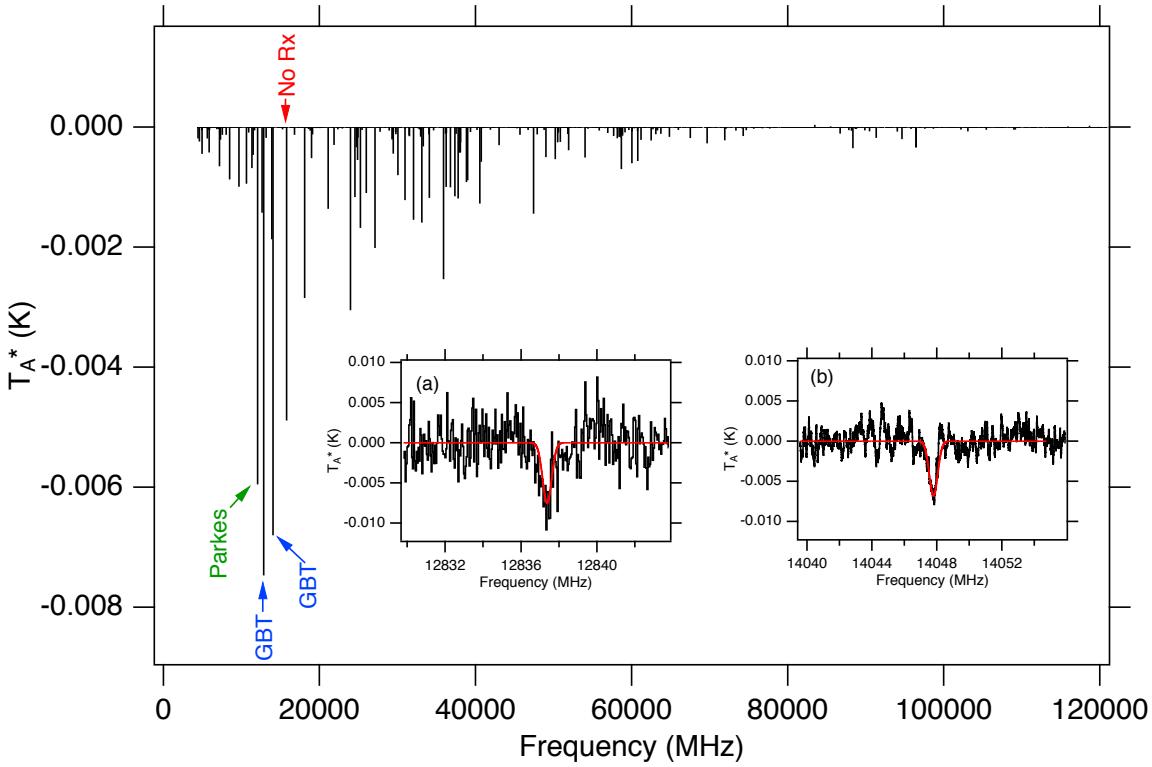

Figure S3. Model spectrum of propylene oxide toward Sgr B2(N) at the best-fit column density and temperature, and comparison with observations. The spectrum of propylene oxide at $N_T = 1 \times 10^{13}$ cm^{-2} and $T_{ex} = 5.2$ K, corrected for background continuum, telescope-specific parameters, and beam dilution effects is shown in the main figure. The observed transitions in PRIMOS are shown in insets (a) and (b), with the model spectra overlaid in red. The next strongest transition has no corresponding receiver (Rx) at the GBT or Parkes, and is marked as such.

The uncertainties for the Gaussian-fitted parameters given in Table S2 are not the dominant source of uncertainty in our analysis. To quantitatively determine the uncertainty in the column density and excitation temperature, we have followed the approach of (*37*), which takes into account uncertainty in the baseline offset, the local rms noise level, the absolute flux calibration, the pointing error, error in the beam filling factor due to uncertainty in the source size, and, in our case, the uncertainty in the determined continuum level. We make conservative estimates of these quantities in our analysis, and assume a 20% uncertainty in the absolute flux calibration,

$2''$ uncertainty in the pointing, a 20% uncertainty in the source size, and a 20% uncertainty in the continuum level. Given the sparsity of spectral features, we assume no contribution to the error from the removal of the baseline.

Given these uncertainties, and combined with the two fitted transitions from PRIMOS, there are a range of models which fit the observed transitions, and non-detected transitions, nearly as well spanning excitation temperatures as high as $\sim$35 K. Nevertheless, a column density of 1×10^{13} cm^{-2} and an excitation temperature of $T_{ex} = 5.2$ K are indeed the best-fit to our observations, although there are a wide range of models which remain consistent with both the detected and non-detected lines from our observations and those with the MOPRA telescope (*10*).

Astronomical Statistical Analysis

The low line density in the cm-wave region of the spectrum allows for the definitive identification of new molecules from far fewer transitions than are required in the (sub-)mm region. This is especially true in the case of Sgr B2(N), where at frequencies $>$100 GHz, broad line-widths, high degrees of molecular-complexity, and large column densities contribute to an essentially baseline-free, completely line-confused spectrum. To illustrate the relative line densities of these two frequency regimes, we have compared our PRIMOS observations around 13 GHz to a selection of spectra toward Sgr B2(N) from the Barry E. Turner Legacy survey taken with the NRAO 12 m telescope on Kitt Peak (accessible at http://www.cv.nrao.edu/$\sim$aremijan/PRIMOS). The frequency windows were chosen to provide equivalent coverage in velocity space ($\sim$6000 km s^{-1}) in both scans.

In the Turner Survey, which has an RMS of $\sim$14 mK, there are $\sim$315 lines at 3σ or above, with a resulting line density of $\sim$1 line per 10 MHz ($\sim$1 line per 20 km s^{-1}). Herschel HIFI

and ALMA data have even lower noise floors and are essentially line-confusion limited at all frequencies. Typical linewidths in this source are 8 – 25 km s^{-1} FWHM, making significant line blending inevitable (*11, 16, 30, 32*). To claim a detection of a line in the presence of blending, however, the components must be separated by at least their FWHM (*38*), and the coincidence of lines separated by this criterion is greatly reduced in such crowded spectra. Thus detections at (sub-)mm wavelengths regularly require dozens or hundreds of lines to be secure, and fitting techniques must explicitly account for line blending.

In the PRIMOS survey, there are $\sim$26 lines above 3σ in the same $\sim$6000 km s^{-1} window, resulting in a similar line density of $\sim$1 line per 10 MHz in frequency space. In velocity space, however, the line density drops to $\sim$1 line per 230 km s^{-1}. With an average line separation > 10 times the linewidth, there is almost no chance for coincidental overlap. Thus as long as the assignments of laboratory spectra are robust, molecular detections at cm wavelengths require only a few (2 – 5) lines to be secure.

The lack of line confusion in the PRIMOS survey allows for further quantitative constraints on the likelihood of a spurious detection (*13*). Previous observations gave a propylene oxide column density upper limit of $\leq 6.7 \times 10^{14}$ cm^{-2}, so we may conservatively only consider features between -100 mK and $+100$ mK. If we further restrict ourselves to only absorption features, as would be expected for a rotationally cold molecule toward a strong background source, the number of candidate features is $\sim$ 0.28 per 10 MHz. For this line density, the probability of finding a feature coincident with a propylene oxide transition rest frequency, defined conservatively as being within twice the largest source FWHM, 50 km s^{-1} (2.2 MHz), is $\sim$ 0.06. The likelihood of three such coincidences is then $\sim 2 \times 10^{-4}$.

The high resolution of our observations provides even further constraint, as all three observed transition peaks fall within 3 resolution elements (73.2 kHz or 1.7 km s^{-1}) of the measured laboratory transition frequency. For the given line density, the likelihood of a single

coincident transition falling no more than 73.2 kHz from the rest frequency is ~ 0.004, and the likelihood of three transitions all occurring within this window is $\sim 6 \times 10^{-8}$.

Finally, although a wide range of linewidths are observed toward Sgr B2(N), the two transitions measured with the GBT show nearly identical linewidths, providing further evidence that the transitions are truly related, and are not spurious. As previously noted, the Parkes data samples a substantially different total population and its linewidth cannot be directly compared.

Measurement of Circular Dichroism

The most straightforward method available for astronomical detection of e.e. is circular dichroism. Circular dichroism (CD), or preferential absorption of left- or right-handed circularly polarized light (CPL) manifests itself as a change in the difference in the electric field of left versus right-handed CPL, commonly referred to as the Stokes V parameter, that follows the absorption profile of the observed (in this case, propylene oxide) features. In principle, detection of e.e. requires two CD measurements. First, is a quantitative laboratory measurement of CD to relate e.e. to an observed CD. Second, and most critically, is a polarization-sensitive astronomical observation to detect CD.

For laboratory measurements, this requires experimental measurement and quantification of CD for each of the transitions in question. In the present case this would require laboratory absorption measurement of CD for the cm-wave propylene oxide transitions at 12.1,12.8, and 14.0 GHz. To date, CD has been shown in a laboratory setting from the ultraviolet to the mid-infrared. Extension to the microwave, or radio region, has been studied theoretically (*39*). These studies conclude that such measurements should be feasible, although they have not yet been experimentally demonstrated. Such measurements would then enable quantitative analysis of polarization-sensitive astronomical observations of CD discussed below.

Modern radio telescopes, especially unblocked off-axis designs such as the GBT, are capable

of highly-accurate, polarization-sensitive observations across wide frequency windows, simultaneously determining the polarization state at each observed frequency (e.g. (*40*)). Briefly, this is achieved by using receivers that simultaneously detect the electric field of two orthogonal polarizations. The in-phase (0°) and quadrature-phase (90°) components of the electric field for each polarization are then separated and digitized. Appropriate combinations of these four signals are then used to fully determine the polarization state at each frequency within the observed pass band, producing a Stokes vector (discussed below) at each frequency. Acquiring accurate, phase-calibrated, data across large pass bands requires careful calibration, but is regularly achieved by properly designed radio receivers (*41*). Such observations are vital both for detection of circular dichroism and to distinguish other effects that may change the polarization state of the detected light, obfuscating potential CD signals.

In astronomical observations, there are two potential sources of confusion for the detection of circular dichroism: non-resonant effects, i.e. those that do not require light at a frequency corresponding to transitions between states of a molecule, and resonant effects that do. First are macroscopic or non-resonant effects, e.g. Faraday rotation or dust scattering. For such effects, small changes in frequency produce effectively no difference in the effect on the polarization (*42*). In the present observations, the linewidth is $\sim$ 700 kHz, at frequencies of several GHz, making the difference between on and off resonance is extremely small ($\sim 10^{-5}$). Therefore any non-resonant effect that alters the polarization at the frequency of the absorption will have the same effect in non-absorption channels and this effect can be corrected by comparison of the polarization on and off resonance.

The second possible source of confusion is resonant effects. Because resonant effects are specific not only to a molecule, but to a transition between states of a particular molecule, they occur only in the narrow region where a molecule absorbs or emits. Effects that produce changes in linear polarization, e.g. the Goldreich-Kylafis effect (*43*), are readily distinguished

from circular dichroism, as they produce changes in linear, rather than circular polarization, which is distinct from CD. The plausible effect other than circular dichroism to produce changes in circularly polarized light is the Zeeman effect. In this scenario an applied magnetic field lifts the degeneracy of the m sublevels, and positive m sublevels interact preferentially with one handed of circularly polarized light, while negative m sublevels interact with the opposite handedness. This too is easily distinguished from circular dichroism. In order to produce non-canceling circular polarization, the Zeeman splitting must be spectrally-resolved. Spectrally-resolved Zeeman splitting produces distinct peaks with circular polarizations of opposite sign. Conversely, circular dichroism produces a single peak of a single sign (*39, 44*).

Furthermore, observing a wide bandwidth allows for additional tests to prevent false positives and constrain polarization effects. By observing one of several achiral species originating from the same region as propylene oxide, e.g. propanal or acetone, it can be confirmed that there are no resonant molecular effects or observational artifacts causing changes in the polarization. Higher order effects such as the Cotton-Mouton effect, quadratic field induced optical activity, and the magnetochiral effect scale nonlinearly with static magnetic field and given the modest measured field strengths toward Sgr B2(N), are not considered (*45, 46*).

For astronomical observations, it is then critical to demonstrate that CD produces observable polarization effects that are distinct from other potential effects, and is therefore an astronomically observable effect. The polarization state of light can be completely specified by four parameters, commonly chosen to be the four Stokes parameters, I, Q, U, and V, where I is the total intensity, Q is linear polarization, U is 45° linear polarization, and V is circular polarization. This is often written as a vector $\mathbf{S}$ = [I,U,Q,V]. Using these vectors, any polarization-altering effect may evaluated using the so-called Mueller matrices (*47*). For on and off-resonance observations, the polarization vectors will be of the form $\mathbf{V}' = \mathbf{M}_{los} \cdot \mathbf{V}$, where $\mathbf{V}$ is some initial Stokes vector, $\mathbf{M}_{los}$ is a Mueller matrix describing subsequent polarization changes along the

line of sight, and $\mathbf{V}'$ is the Stokes vector measured by the telescope. In the absence of CD, the Stokes vector is exactly as above, while on resonance and additional term describing CD must be included. The resulting vector is then given by $\mathbf{V}'' = \mathbf{M}_{los} \cdot \mathbf{M}_{CD} \cdot \mathbf{V}$. The difference between on and off resonance observations, $\mathbf{V}''$-$\mathbf{V}'$, is given by $\mathbf{M}_{los} \cdot \mathbf{V}$-$\mathbf{M}_{los} \cdot \mathbf{M}_{CD} \cdot \mathbf{V} = \mathbf{M}_{los}$(V-$\mathbf{M}_{CD} \cdot \mathbf{V}$). If these two vectors are identical the difference is zero, and they indistinguishable, as is the effect of circular dichroism. This expression is zero for two conditions, if the kernel of $\mathbf{M}_{los}$ is not null, or if $\mathbf{V}$ is an eigenvector of $\mathbf{M}_{CD}$, with eigenvalue 1. The first condition can only be met if the line-of-sight transmittance is zero, i.e. if there is complete absorption along the line of sight. For the second condition $\mathbf{M}_{CD}$ has eigenvectors [1,0,0,1], [0,1,0,0], [0,0,1,0], [1,0,0,-1] (*47*). Of these four vectors, only two can be physically meaningful, corresponding to the pure circularly polarized states. $\mathbf{M}_{CD}$ has eigenvalue 1 only for complete transmittance. The result is that the only valid eigenvector for $\mathbf{M}_{CD}$ with eigenvalue 1 is completely transmitted pure circular polarization. Thus the only two cases in which the on and off resonance Stokes vectors are indistinguishable are total absorption or the absence of any CD, meaning that CD must produce a distinct Stokes vector.

From this analysis it is clear that observations at a frequency where CD occurs and where it does not must produce distinct results, and careful measurements may thus identify CD in observations. In the case of the present observations however, a meaningful measurement of the Stokes vector is not possible. This is principally due to a lack of polarization calibration. Even extremely well-designed receivers such as those at the GBT, may introduce significant polarization artifacts through a variety of effects, including polarization side lobes, beam squint, and non-orthogonal response (*41*). These effects have dependence on frequency, position angle throughout observations, altitude and azimuth coordinates of the dish, and even cable length, and therefore necessitate great care to accurately determine Stokes vectors and prevent detection of spurious polarization effects.

Propanal and Acetone Observations in PRIMOS

We have examined the PRIMOS dataset for transitions of acetone and propanal. We find 18 clear, unblended transitions of acetone (Table S3), and 11 similarly distinct transitions of propanal (Table S4). All transitions were observed in absorption, and parameters derived by single-Gaussian fits to the lines were determined. We use the method described above to fit a column density and temperature to these species using these observed transitions, but note that we make no effort to refine the physical models from those used for propylene oxide. A static linewidth of 12 km s^{-1} was used for acetone, and a linewidth of 9 km s^{-1} for propanal. The source size was taken as $20''$ in both cases.

The models derived here reproduce the observed intensities to within a factor of $\sim$2 (Figures S4 and S5), and the uncertainties in these parameters should be taken to be of this order. Further, for acetone in particular, a warm component is known to be present within the PRIMOS beam, but was not explicitly treated in this analysis. Thus, while the derived values are useful for qualitative comparisons with each other and propylene oxide, a more rigorous treatment than the single population, single excitation-temperature model used here, although beyond the scope of this work, would refine the results.

Table S3. Observed acetone transitions in PRIMOS.

$J'_{K_a,K_c} - J''_{K_a,K_c}$	Frequency (MHz)	ΔT_A^* (mK)	ΔV (km s^{-1})
$3_{2,1} - 3_{1,2}$ AE	10731.360(9)	-33.0(9)	16.5(6)
$4_{3,1} - 4_{2,2}$ EE	11569.943(4)	-60(3)	14.9(9)
$4_{3,1} - 4_{2,2}$ EA	11583.080(5)	-13(3)	10(3)
$4_{3,1} - 4_{2,2}$ AA	11585.245(3)	-11(2)	10(3)
$5_{4,1} - 5_{3,2}$ EE	14263.975(5)	-28.7(8)	15.8(6)
$5_{4,1} - 5_{3,2}$ AA	14276.816(6)	-18.6(7)	14.8(9)
$4_{2,2} - 4_{1,3}$ EE	18654.309(4)	-29.7(8)	12.7(4)
$3_{1,2} - 3_{0,3}$ AA	20454.895(4)	-9(1)	12(2)
$3_{2,2} - 3_{1,3}$ EE	22413.051(3)	-12.2(5)	8.8(4)
$2_{0,2} - 1_{1,1}$ AA	22793.262(3)	-7.5(7)	12(2)
$2_{0,2} - 1_{1,1}$ EE	22800.382(2)	-32.2(7)	11.8(3)
$4_{3,2} - 4_{2,3}$ EE	23469.238(4)	-18.4(7)	12.2(5)
$4_{3,2} - 4_{2,3}$ AA	23549.025(4)	10.7(9)	10.7(9)
$2_{1,2} - 1_{0,1}$ AA	24916.487(3)	-7.3(9)	9(1)
$3_{1,3} - 2_{0,2}$ EE	34092.973(3)	-23(2)	11.6(9)
$2_{2,1} - 1_{1,0}$ AE	35371.432(5)	-13(2)	8(1)
$2_{2,1} - 1_{1,0}$ EE	35381.289(4)	-43(1)	17.8(7)
$2_{2,1} - 1_{1,0}$ AA	35468.174(5)	-22(2)	6.8(9)

Numbers in parentheses are 1σ uncertainties in units of the last significant digit. A and E labels designate torsional sub-levels.

Table S4. Observed propanal transitions in PRIMOS.

$J'_{K_a,K_c} - J''_{K_a,K_c}$	Frequency (MHz)	ΔT_A^* (mK)	ΔV (km s^{-1})
$2_{0,2} - 1_{1,1}$	10098.84(5)	-14.3(8)	21(1)
$4_{1,3} - 4_{0,4}$	19182.410(4)	-8.3(8)	5.8(8)
$2_{1,2} - 1_{1,1}$	19690.51(5)	-18.2(4)	10.2(3)
$2_{0,2} - 1_{0,1}$	20875.19(5)	-8.6(5)	8.7(5)
$3_{0,3} - 2_{1,2}$	21451.62(5)	-17.0(7)	9.0(4)
$2_{1,1} - 1_{1,0}$	22279.26(5)	-8.6(9)	3.8(4)
$4_{2,2} - 4_{1,3}$	29618.95(5)	-28(1)	13.8(9)
$3_{2,1} - 3_{1,2}$	31002.20(5)	-13(2)	6.8(9)
$4_{0,4} - 3_{1,3}$	32897.82(5)	-13(2)	6(1)
$3_{1,3} - 2_{0,2}$	39061.03(5)	-21(1)	10.6(8)
$4_{1,4} - 3_{1,3}$	39177.132(5)	-20(1)	12(2)

Numbers in parentheses are 1σ uncertainties in units of the last significant digit.

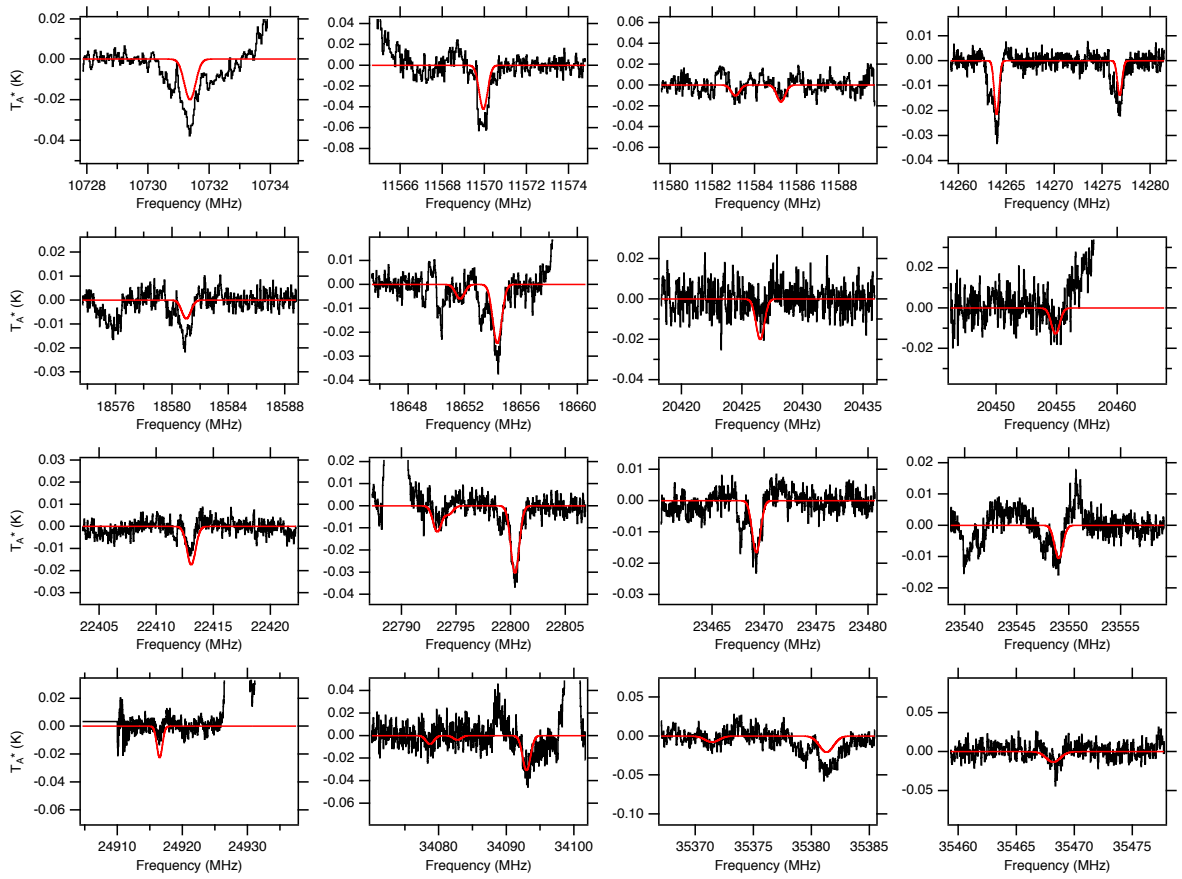

Figure S4. Model spectrum of acetone toward Sgr B2(N) at the best-fit column density and temperature, and comparison with observations. The spectrum of acetone at $N_T = 2.1\times10^{14}$ cm^{-2} and $T_{ex} = 6.2$ K, corrected for background continuum, telescope-specific parameters, and beam dilution effects is shown in the main figure. The observed transitions in PRIMOS are shown in black, with the model spectra overlaid in red.

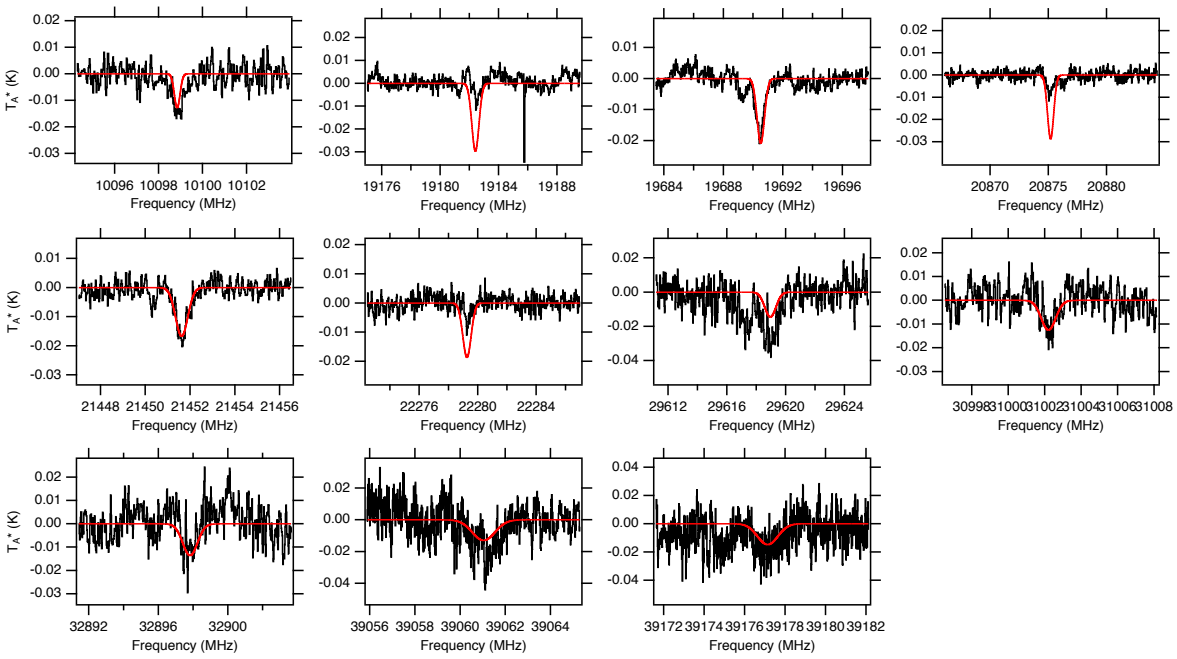

Figure S5. Model spectrum of propanal toward Sgr B2(N) at the best-fit column density and temperature, and comparison with observations. The spectrum of propanal at $N_T = 6 \times 10^{13}$ cm^{-2} and $T_{ex} = 6.2$ K, corrected for background continuum, telescope-specific parameters, and beam dilution effects is shown in the main figure. The observed transitions in PRIMOS are shown in black, with the model spectra overlaid in red.

References

1. S. Pizzarello, T. L. Groy, Molecular asymmetry in extraterrestrial organic chemistry: An analytical perspective. *Geochim. Cosmochim. Acta* **75**, 645–656 (2011). doi:10.1016/j.gca.2010.10.025

2. J. Lunine, *Astrobiology: A Multi-Disciplinary Approach* (Pearson Education Inc., San Francisco, CA, 2005).

3. M. H. Engel, S. A. Macko, Isotopic evidence for extraterrestrial non-racemic amino acids in the Murchison meteorite. *Nature* **389**, 265–268 (1997). Medline doi:10.1038/38460

4. D. P. Glavin, J. P. Dworkin, Enrichment of the amino acid L-isovaline by aqueous alteration on CI and CM meteorite parent bodies. *Proc. Natl. Acad. Sci. U.S.A.* **106**, 5487–5492 (2009). Medline doi:10.1073/pnas.0811618106

5. L. I. Cleeves, E. A. Bergin, C. M. Alexander, F. Du, D. Graninger, K. I. Öberg, T. J. Harries, The ancient heritage of water ice in the solar system. *Science* **345**, 1590–1593 (2014). Medline doi:10.1126/science.1258055

6. C. F. Chyba, P. J. Thomas, L. Brookshaw, C. Sagan, Cometary delivery of organic molecules to the early Earth. *Science* **249**, 366–373 (1990). Medline doi:10.1126/science.11538074

7. J. L. Neill, M. T. Muckle, D. P. Zaleski, A. L. Steber, B. H. Pate, V. Lattanzi, S. Spezzano, M. C. McCarthy, A. J. Remijan, Laboratory and tentative interstellar detection of trans-methyl formate using the publicly available Green Bank Telescope PRIMOS survey. *Astrophys. J.* **755**, 153 (2012). doi:10.1088/0004-637X/755/2/153

8. Materials and methods are available as supplementary materials on *Science* Online.

9. P. A. Jones, M. G. Burton, M. R. Cunningham, K. M. Menten, P. Schilke, A. Belloche, S. Leurini, J. Ott, A. J. Walsh, Spectral imaging of the Sagittarius B2 region in multiple 3-mm molecular lines with the Mopra telescope. *Mon. Not. R. Astron. Soc.* **386**, 117–137 (2008). doi:10.1111/j.1365-2966.2008.13009.x

10. M. R. Cunningham, P. A. Jones, P. D. Godfrey, D. M. Cragg, I. Bains, M. G. Burton, P. Calisse, N. H. M. Crighton, S. J. Curran, T. M. Davis, J. T. Dempsey, B. Fulton, M. G. Hidas, T. Hill, L. Kedziora-Chudczer, V. Minier, M. B. Pracy, C. Purcell, J. Shobbrook, T. Travouillon, A search for propylene oxide and glycine in Sagittarius B2 (LMH) and Orion. *Mon. Not. R. Astron. Soc.* **376**, 1201–1210 (2007). doi:10.1111/j.1365-2966.2007.11504.x

11. J. M. Hollis, P. R. Jewell, F. J. Lovas, A. Remijan, Green Bank Telescope Observations of interstellar glycolaldehyde: Low-temperature sugar. *Astrophys. J.* **613**, L45–L48 (2004). doi:10.1086/424927

12. B. A. McGuire, R. A. Loomis, C. M. Charness, J. F. Corby, G. A. Blake, J. M. Hollis, F. J. Lovas, P. R. Jewell, A. J. Remijan, Interstellar carbodiimide (HNCNH): A new astronomical detection from the GBT PRIMOS survey via maser emission features. *Astrophys. J.* **758**, L33 (2012). doi:10.1088/2041-8205/758/2/L33

13. J. M. Hollis, P. R. Jewell, F. J. Lovas, A. Remijan, H. Møllendal, Green Bank Telescope detection of new interstellar aldehydes: Propenal and propanal. *Astrophys. J.* **610**, L21–L24 (2004). doi:10.1086/423200

14. M. A. Requena-Torres, J. Martín-Pintado, A. Rodríguez-Franco, S. Martín, N. J. Rodríguez-Fernández, P. de Vicente, Organic molecules in the Galactic center. *Astron. Astrophys.* **455**, 971–985 (2006). doi:10.1051/0004-6361:20065190

15. M. Ikeda, M. Ohishi, A. Nummelin, J. E. Dickens, P. Bergman, A. Hjalmarson, W. M. Irvine, Survey observations of c-C_2H_4O and CH_3CHO toward massive star-forming regions. *Astrophys. J.* **560**, 792–805 (2001). doi:10.1086/322957

16. R. A. Loomis, D. P. Zaleski, A. L. Steber, J. L. Neill, M. T. Muckle, B. J. Harris, J. M. Hollis, P. R. Jewell, V. Lattanzi, F. J. Lovas, O. Martinez Jr., M. C. McCarthy, A. J. Remijan, B. H. Pate, J. F. Corby, The detection of interstellar ethanimine (CH_3CHNH) from observations taken during the GBT PRIMOS survey. *Astrophys. J.* **765**, L9 (2013). doi:10.1088/2041-8205/765/1/L9

17. L. E. Snyder, F. J. Lovas, D. M. Mehringer, N. Y. Miao, Y.-J. Kuan, J. M. Hollis, P. R. Jewell, Confirmation of interstellar acetone. *Astrophys. J.* **578**, 245–255 (2002). doi:10.1086/342273

18. J. E. Dickens, W. M. Irvine, M. Ohishi, M. Ikeda, S. Ishikawa, A. Nummelin, A. Hjalmarson, Detection of interstellar ethylene oxide (c-C_2H_4O). *Astrophys. J.* **489**, 753–757 (1997). Medline doi:10.1086/304821

19. A. Belloche, H. S. P. Müller, K. M. Menten, P. Schilke, C. Comito, Complex organic molecules in the interstellar medium: IRAM 30 m line survey of Sagittarius B2(N) and (M). *Astron. Astrophys.* **559**, A47 (2013). doi:10.1051/0004-6361/201321096

20. A. Lifshitz, C. Tamburu, Isomerization and decomposition of propylene oxide. Studies with a single-pulse shock tube. *J. Phys. Chem.* **98**, 1161–1170 (1994). doi:10.1021/j100055a020

21. E. Herbst, E. F. van Dishoeck, Complex organic interstellar molecules. *Annu. Rev. Astron. Astrophys.* **47**, 427–480 (2009). doi:10.1146/annurev-astro-082708-101654

22. R. A. Loomis, B. A. McGuire, C. Shingledecker, C. H. Johnson, S. Blair, A. Robertson, A. J. Remijan, Investigating the minimum energy principle in searches for new molecular species—The case of H_2C_3O isomers. *Astrophys. J.* **799**, 34 (2015). doi:10.1088/0004-637X/799/1/34

23. F. Goesmann, H. Rosenbauer, J. H. Bredehoft, M. Cabane, P. Ehrenfreund, T. Gautier, C. Giri, H. Kruger, L. Le Roy, A. J. MacDermott, S. McKenna-Lawlor, U. J. Meierhenrich, G. M. M. Caro, F. Raulin, R. Roll, A. Steele, H. Steininger, R. Sternberg, C. Szopa, W. Thiemann, S. Ulamec, Organic compounds on comet 67P/Churyumov-Gerasimenko revealed by COSAC mass spectrometry. *Science* **349**, aab0689 (2015). doi:10.1126/science.aab0689

24. P. Modica, C. Meinert, P. de Marcellus, L. Nahon, U. J. Meierhenrich, L. L. S. d'Hendecourt, Enantiomeric excesses induced in amino acids by ultraviolet circularly polarized light irradiation of extraterrestrial ice analogs: A possible source of asymmetry for prebiotic chemistry. *Astrophys. J.* **788**, 79 (2014). doi:10.1088/0004-637X/788/1/79

25. J. M. Dreiling, T. J. Gay, Chirally sensitive electron-induced molecular breakup and the Vester-Ulbricht hypothesis. *Phys. Rev. Lett.* **113**, 118103 (2014). Medline doi:10.1103/PhysRevLett.113.118103

26. J. Bailey, A. Chrysostomou, J. H. Hough, T. M. Gledhill, A. McCall, S. Clark, F. Ménard, M. Tamura, Circular polarization in star-formation regions: Implications for biomolecular homochirality. *Science* **281**, 672–674 (1998). doi:10.1126/science.281.5377.672

27. J. D. Swalen, D. R. Herschbach, Internal barrier of propylene oxide from the microwave spectrum. I. *J. Chem. Phys.* **27**, 100 (1957). doi:10.1063/1.1743645

28. D. R. Herschbach, J. D. Swalen, Internal barrier of propylene oxide from the microwave spectrum. II. *J. Chem. Phys.* **29**, 761 (1958). doi:10.1063/1.1744588

29. I. A. Finneran, D. B. Holland, P. B. Carroll, G. A. Blake, A direct digital synthesis chirped pulse Fourier transform microwave spectrometer. *Rev. Sci. Instrum.* **84**, 083104 (2013). doi:10.1063/1.4818137

30. D. P. Zaleski, N. A. Seifert, A. L. Steber, M. T. Muckle, R. A. Loomis, J. F. Corby, O. Martinez Jr., K. N. Crabtree, P. R. Jewell, J. M. Hollis, F. J. Lovas, D. Vasquez, J. Nyiramahirwe, N. Sciortino, K. Johnson, M. C. McCarthy, A. J. Remijan, B. H. Pate, Detection of E-cyanomethanimine toward Sagittarius B2(N) in the Green Bank Telescope PRIMOS survey. *Astrophys. J.* **765**, L10 (2013). doi:10.1088/2041-8205/765/1/L10

31. W. Gordy, R. L. Cook, *Microwave Molecular Spectra* (Wiley, New York, ed. 3 1984).

32. J. M. Hollis, A. J. Remijan, P. R. Jewell, F. J. Lovas, Cyclopropenone (c-H_2C_3O): A new interstellar ring molecule. *Astrophys. J.* **642**, 933–939 (2006). doi:10.1086/501121

33. C. H. Townes, *Microwave Spectroscopy* (Dover Publications, New York, 1975).

34. J. M. Hollis, P. R. Jewell, A. J. Remijan, F. J. Lovas, Nonthermal continuum toward Sagittarius B2(N-LMH). *Astrophys. J.* **660**, L125–L128 (2007). doi:10.1086/518124

35. N. Ladd, C. Purcell, T. Wong, S. Robertson, Beam size, shape and efficiencies for the ATNF Mopra Radio Telescope at 86–115 GHz. *Publ. Astron. Soc. Aust.* **22**, 62–72 (2005). doi:10.1071/AS04068

36. D. M. Mehringer, P. Palmer, W. M. Goss, F. Yusef-Zadeh, Radio continuum and radio recombination line observations of Sagittarius B2. *Astrophys. J.* **412**, 684 (1993). doi:10.1086/172954

37. N. R. Crockett, E. A. Bergin, J. L. Neill, C. Favre, P. Schilke, D. C. Lis, T. A. Bell, G. Blake, J. Cernicharo, M. Emprechtinger, G. B. Esplugues, H. Gupta, M. Kleshcheva, S. Lord, N. Marcelino, B. A. McGuire, J. Pearson, T. G. Phillips, R. Plume, F. van der Tak, B. Tercero, S. Yu, Herschel observations of extraordinary sources: Analysis of the HIFI 1.2 THz wide spectral survey toward Orion KL. I. Methods. *Astrophys. J.* **787**, 112 (2014). doi:10.1088/0004-637X/787/2/112

38. L. Snyder, F. J. Lovas, J. M. Hollis, D. N. Friedel, P. R. Jewell, A. Remijan, V. V. Ilyushin, E. A. Alekseev, S. F. Dyubko, A rigorous attempt to verify interstellar glycine. *Astrophys. J.* **619**, 914–930 (2005). doi:10.1086/426677

39. W. R. Salzman, Circular dichroism at microwave frequencies: Calculated rotational strengths for transitions up to $J = 10$ for some oxirane derivatives. *J. Mol. Spectrosc.* **192**, 61–68 (1998). Medline doi:10.1006/jmsp.1998.7677

40. B. S. Mason, T. Robishaw, C. Heiles, D. Finkbeiner, C. Dickinson, A limit on the polarized anomalous microwave emission of Lynds 1622. *Astrophys. J.* **697**, 1187–1193 (2009). doi:10.1088/0004-637X/697/2/1187

41. T. Robishaw, C. Heiles, On measuring accurate 21 cm line profiles with the Robert C. Byrd Green Bank Telescope. *Publ. Astron. Soc. Pac.* **121**, 272–294 (2009). doi:10.1086/597985

42. B. T. Draine, *Physics of the Interstellar and Intergalactic Medium* (Princeton Univ. Press, 2011).

43. P. Goldreich, N. D. Kylafis, On mapping the magnetic field direction in molecular clouds by polarization measurements. *Astrophys. J. Lett.* **243**, L75 (1981). doi:10.1086/183446

44. T. Robishaw, E. Quataert, C. Heiles, Extragalactic Zeeman detections in OH megamasers. *Astrophys. J.* **680**, 981–998 (2008). doi:10.1086/588031

45. G. H. Wagnière, The magnetochiral effect and related optical phenomena. *Chem. Phys.* **245**, 165–173 (1999). doi:10.1016/S0301-0104(99)00023-3

46. R. M. Crutcher, D. A. Roberts, D. M. Mehringer, T. H. Troland, H I Zeeman measurements of the magnetic field in Sagittarius B2. *Astrophys. J. Lett.* **462**, L79 (1996). doi:10.1086/310031

47. M. Bass *et al*., *Handbook of Optics, Third Edition, Volume I: Geometrical and Physical Optics, Polarized Light, Components and Instruments (Set)* (McGraw-Hill, Inc., ed. 3, New York, NY, USA, 2010).